

© 2010 Arash Sayyah

OPTIMIZATION OF PERMANENT MAGNET BRUSHLESS MACHINE  
FOR BIOMECHANICAL ENERGY HARVESTING APPLICATIONS

BY

ARASH SAYYAH

THESIS

Submitted in partial fulfillment of the requirements  
for the degree of Master of Science in Electrical and Computer Engineering  
in the Graduate College of the  
University of Illinois at Urbana-Champaign, 2010

Urbana, Illinois

Adviser:

Associate Professor Patrick L. Chapman

# ABSTRACT

For electrical power generation over long durations, it would be desirable to harvest energy normally wasted during ordinary human activities such as walking. It is a challenge, however, to produce substantial electricity from walking. Most energy harvesting research has concentrated on generating electricity from the compression of the shoe sole, with the best devices generating 0.8 W, reported by Paradiso (2005).

This thesis addresses a noteworthy departure, which is a spring-loaded backpack that harnesses the vertical movements of a load to generate electricity during normal walking. A mechanical apparatus can be used to convert the linear motion to a rotary one. Based on characteristics of the motion, a brushless permanent magnet generator is chosen as the candidate for this energy conversion rather than the linear permanent magnet generator used previously in the literature.

The split ratio, i.e. the ratio of the stator bore diameter to the stator outer diameter, is considered as one of the important parameters in designing cylindrical permanent magnet brushless machines. The objective function of motor constant per unit volume is studied in this work. The optimal split ratio is investigated analytically for motors having overlapping and non-overlapping windings, and accounting for the influence of the air gap flux distribution, the stator tooth-tips and the end-windings. It is shown that the split ratio can notably influence the motor constant (i.e. torque efficiency) of a permanent magnet brushless motor.

*To my parents, for their unconditional love and support*



# ACKNOWLEDGMENTS

First and foremost, I would like to express my profound gratitude to my supervisor, Professor Patrick L. Chapman, for his continued encouragement, support and supervision which brought about a pleasant academic life for me at the University of Illinois. Without his sincere help, I would not have come this far.

I owe an immense debt to my parents for encouraging and consistently supporting my endeavors throughout my life. Without their sincere support, graduate school at one of the finest universities in the world would have seemed an unachievable dream. Furthermore, I am greatly thankful to all my friends for all their kindness.

# TABLE OF CONTENTS

LIST OF FIGURES . . . . .	vi
LIST OF ABBREVIATIONS . . . . .	vii
LIST OF SYMBOLS . . . . .	viii
CHAPTER 1 INTRODUCTION . . . . .	1
1.1 Fuel Cell . . . . .	1
1.2 Piezoelectric Materials . . . . .	2
1.3 Biomechanical Energy . . . . .	4
1.4 Outline of the Thesis . . . . .	7
CHAPTER 2 BRUSHLESS PERMANENT MAGNET MOTOR . . . . .	8
2.1 Assumptions . . . . .	8
2.2 Magnetic Circuit Model . . . . .	9
2.3 Magnetic Circuit Solution . . . . .	11
2.4 Flux Linkage, Back EMF, and Torque . . . . .	12
CHAPTER 3 MOTOR CONSTANT OPTIMIZATION . . . . .	15
3.1 Optimization of Motor Constant per Unit Volume . . . . .	15
3.2 Influence of Winding Disposition on Optimal Split Ratio . . . . .	18
3.3 Influence of Tooth-Tips on Optimal Split Ratio . . . . .	20
3.4 Influence of End-Windings on Optimal Split Ratio . . . . .	23
CHAPTER 4 CONCLUSION . . . . .	31
REFERENCES . . . . .	33
AUTHOR'S BIOGRAPHY . . . . .	35

# LIST OF FIGURES

1.1	Fuel cells convert fuel into electric current [5]. . . . .	2
1.2	Using piezoelectric materials under the heel in heel-strike movement [9]. . . . .	3
1.3	Simple model of the biomechanical energy harvester [18]. . . .	6
2.1	Fundamental motor structure and associated flux paths. . . .	9
2.2	A magnetic circuit model for the structure shown in Figure 2.1.	10
2.3	Simplifications of the magnetic circuit in Figure 2.2. . . . .	11
2.4	Motor having one full-pitch coil. . . . .	12
2.5	Flux linkage as a function of rotor position. . . . .	13
3.1	Variation of optimal split ratio $B_g/B_{max}$ for motor with non-overlapping winding. . . . .	18
3.2	Variation of optimal split ratio with number of pole-pairs and winding disposition. . . . .	20
3.3	Idealized stator slot shape. . . . .	21
3.4	Influence of height of tooth tips on optimal split ratio $p = 2$ , $D_o = 90$ mm, non-overlapping winding. . . . .	23
3.5	Influence of tooth-tips and end-winding on optimal split ratio. $p = 2$ , $N_s = 6$ , $D_o = 90$ mm, $l_a = 50$ mm, non-overlapping winding. . . . .	29
3.6	Influence of tooth-tips and end-winding on optimal split ratio. $p = 2$ , $N_s = 12$ , $D_o = 90$ mm, $l_a = 50$ mm, overlapping winding. . . . .	30

# LIST OF ABBREVIATIONS

AC	alternating current
BPM	brushless permanent magnet
DC	direct current
EMF	electromotive force
MMF	magnetomotive force
PM	permanent magnet
RMS	root mean square value
rad	radians
radM	radians mechanical
rpm	revolutions per minute
°E	degrees electrical
°M	degrees mechanical

# LIST OF SYMBOLS

$A$	area (m <sup>2</sup> )
$A_{cond}$	conductor area (m <sup>2</sup> )
$A_g$	air gap cross-sectional area (m <sup>2</sup> )
$A_m$	magnet cross-sectional area (m <sup>2</sup> )
$A_s$	slot area (m <sup>2</sup> )
$B_g$	air gap flux density (T)
$B_{max}$	maximum flux density in the stator iron (T)
$C_\phi$	flux concentration factor
$D_o$	stator outer diameter (m)
$D_s$	stator bore diameter (m)
$\frac{D_s}{D_o}$	split ratio
$e_{ph}$	amplitude of the phase back-EMF (V)
$g$	air gap length (m)
$H$	magnetic field intensity (A/m)
$h_t$	tooth-tip height (m)
$I, i$	current (A)
$I_a$	RMS phase current (A)
$K_{dp}$	winding factor
$K_e$	back EMF constant (V/rad/s)
$K_l$	magnet leakage factor

$K_m$	motor constant
$K_r$	reluctance factor
$K_s$	slot packing factor
$K_t$	torque constant (N·m/A)
$L$	length (m) inductance (H)
$L_{st}$	axial stack length (m)
$l_a$	active axial length (m)
$l_e$	average total length of the end-windings (m)
$N_s$	number of slots
$N_w$	number of turns per phase
$p$	number of pole-pairs
$R$	reluctance (m/H)
$R_g$	air gap reluctance (m/H)
$R_l$	leakage reluctance (m/H)
$R_m$	magnet air-gap radius (m)
$R_r$	radius to underside of magnet (m)
$R_{ro}$	rotor outside radius (m)
$R_s$	radius to stator-air-gap interface (m)
$T$	torque (N·m)
$V_{wb}$	volume of bare wire in a slot (m <sup>3</sup> )
$\theta_e$	electrical position
$\theta_m$	mechanical position
$\lambda$	flux linkage (Wb)
$\mu$	permeability (H/m)
$\rho$	resistivity ( $\Omega\cdot\text{m}$ )
$\phi$	flux (Wb)

$\phi_g$	air gap flux (Wb)
$\phi_r$	magnet remanent flux (Wb)
$\omega_{elec}$	electrical angular velocity
$\omega_m$	mechanical frequency (rad/s)

# CHAPTER 1

## INTRODUCTION

Over the past years, humans have become notably dependent on technology, specifically portable electronic devices such as cellular phones, navigation systems, music players, cordless devices, and so forth. This growth has caused proliferating need for mobile power delivery. All of the mentioned devices are primarily powered with batteries. Although significant endeavors have been made in increasing the power densities of batteries, battery capacity, weight, temperature sensitivity, and perpetually searching for outlets to recharge them are limiting factors for today's portable devices [1–3]. Lithium is the material used extensively in the battery industry. The major issue of the lithium metal is that it is excessively reactive. Exposing this material to the smallest amount of moisture will cause a fire [4]. In this introduction, we highlight the most significant endeavors with different perspectives that have been proposed from different scholars at companies and research institutes to find a replacement or a backup for batteries.

### 1.1 Fuel Cell

Among the candidate solutions, fuel cells, as shown in Figure 1.1, have received significant attention. Numerous research institutes are studying the commercialization of micro fuel cells, small devices that convert chemical fuels into electrical energy. One of the predominant chemical fuels used in fuel cells is methanol which has around 10 times the energy density of a lithium iron battery. When it comes to powering advanced portable electronics, as R. F. Service has put it, “fuel cells seem to be a front-runner in a field where there are very few choices” [5].

In some applications fuel cells have shown better performance than batteries, but only at higher cost and with excessive private and government



subsidies. It should be pointed out that there are many serious problems associated with using fuel cells at low power levels, although they have maintained their position as the main candidate solutions in some areas like military applications [6]. Miniaturization of fuel cells also faces challenges to its successful commercialization. Most micro fuel cells achieve their optimal performance at high temperatures. Thus, they should be insulated appropriately to prevent damage to the powered electronics. Furthermore, fuel cells, because of the volatility of methanol and other liquid fuels, are not allowed in commercial aircraft. It seems that these devices have a long way to go before they become conventional.

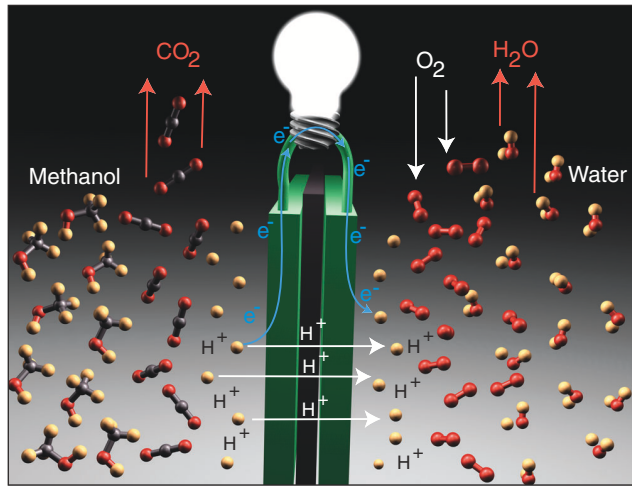


Figure 1.1: Fuel cells convert fuel into electric current [5].

## 1.2 Piezoelectric Materials

Over the past years, numerous research communities have concentrated on discovering and developing new materials and devices to convert ambient energy into electricity. One of the well known approaches for power harvesting is using piezoelectric materials that absorb ambient vibrations. The crystalline structure of these devices endows them with the ability to convert mechanical strain energy into electrical charge and vice versa in order to power other devices [7]. The availability of different kinds of piezoelectric ceramics, single crystals and composites has enabled the production of piezoelectric generators with distinctive geometries.

Using the properties of piezoelectric materials, authors in [1, 8, 9] present three energy conversion devices focused on heel-strike energy harvesting. Two of the devices are piezoelectric actuators, based on complex commercial polyvinylidene fluoride (PVDF) stave and piezoelectric lead zirconate titanate (PZT) unimorph. The piezoelectric devices have been mounted in the sole of a running shoe as shown in Figure 1.2. It is reported that the PVDF stave produced peaks of roughly 60 V with gait speed at roughly 1 Hz, while the PZT unimorph gives a notably higher response, with peaks close to 150 V. Nevertheless, the voltage waveforms of both actuators are shown to be sharp and slim. The recorded average power fed into a large resistive load is 1.1 mW for PVDF stave and 1.8 mW for PZT unimorph.

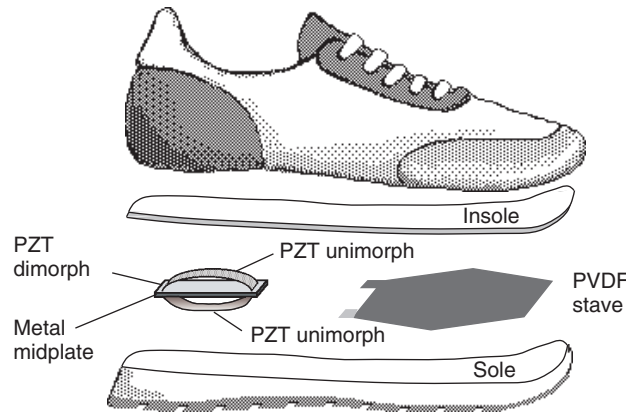


Figure 1.2: Using piezoelectric materials under the heel in heel-strike movement [9].

Most endeavors have been focused on the vertical heel-strike movement. However, the shortcomings of energy scavenging from this motion are noteworthy. In [10], a spring-based heel-strike energy storage device was built and tested. Maximum comfortable displacement under the human heel was reported as 1.27 cm, and the heavy body weight pressing onto the device during the ground reaction threatened the durability of the device.

When piezoelectric materials are used to gather ambient vibration energy, one must include an appropriate electrical interface between the piezoelectric electrodes and the electronic load to put to use the energy produced by the generator. This necessity comes from the fact that the electronic components that may be used for energy storage require DC voltages, whereas the piezoelectric elements produce AC voltages. Furthermore, the desired

outputs may need to be precisely regulated. Without accumulating a noteworthy amount of energy, the power harvesting system will not be a reliable power source for most electronic devices. Several research works [11–13] have utilized circuitry to either store the energy generated by the piezoelectric material or allow the energy to be removed from the piezoelectric efficiently to allow more power to be generated.

Like other research fields, the study of piezoelectric materials for energy harvesting has its own challenges. One of the major constraints is that the generated power is too small to be used by most electronic devices. Thus, both increasing the energy generated by the power harvesting components and more effectively gathering the generated energy are the predominant challenges that should be addressed to make the power harvesting devices reliable sources for portable electronic devices. One promising approach to the later challenge is the use of rechargeable batteries as a means of gathering the generated energy during power harvesting. In initial steps of research on energy harvesting, capacitors played a pivotal role in storing energy and powering electronic devices, but capacitors have shown unfavorable storage characteristics because of their quick discharge time, which causes the electrical output of circuitry to switch on and off as they charge and discharge. The rechargeable battery, however, can be charged and then used to power electronic devices for an extended time.

Moreover, in order to fully utilize the energy transferred from the harvesting device to the storage medium, the efficiency of the electronic circuit should be maximized. Advances in electronics can be utilized not only to maximize the power generated by the piezoelectric device but also to minimize the electronic circuit loss.

### 1.3 Biomechanical Energy

Considering the alternatives described above, we conclude that biomechanical energy, the energy from human motion, is an attractive possible replacement or backup for batteries. Human motion is a notable energy source during which muscles convert food into mechanical work with efficiency of approximately 25% [14]. The work can be performed at a high rate, with a feasible 100 W mechanical by an average person [15]. The original source of the

energy required by muscles is food, which is as rich an energy source as gasoline and approximately 100 times richer than batteries of the same weight [2]. Considering these properties of biomechanical energy, it could be beneficial to utilize an electric generator to convert this produced energy into electrical energy. Some examples are bicycle generators and windup flashlights [16]. Significant advantages of biomechanical energy are that it has no relevant life cycle limitation, is nonpolluting, and does not need recharging like batteries or fuel cartridges like fuel cells, to name a few. It should be pointed out that since biomechanical energy is accessible only during motion (e.g. walking), it should be considered as secondary to conventional power generation, or for use in combination with another appropriate energy supply.

Different motions have been considered as energy sources for biomechanical energy conversion. Heel-strike motion, described above, has received significant attention due to its considerable vertical force. Reference [2] estimated available power from heel-strike as about 67 W. Some of the energetic motions such as heel-strike, however, have been overestimated. In [3], four motions are identified as potential candidates for power generation: heel-strike, joint motion, center-of-mass motion, and horizontal foot movement.

Heel-strike motion has been studied comprehensively as a source of biomechanical energy conversion because a large force comparable with body weight is involved. Based on the observation that the work done during human energetic motions is because of an exchange of potential energy, numerous researchers have considered heel-strike as an ideal candidate motion for energy harvesting. However, energy generation from this motion is overestimated in the literature. The comfortable displacement is quite limited to 1.27 cm. Moreover, a heel-strike device presumably brings much discomfort to normal walking.

Joint motion for energy harvesting has also been considered in research communities. During walking, human limbs swing back and forth, providing motion that can be utilized to generate power. In [17], a wearable knee-mounted energy harvesting device is developed to generate electricity during human walking. The device uses a one-way clutch to transmit knee extension motions, a rotary magnetic generator (brushless DC machine) to convert the mechanical energy into electrical energy, a control system to determine when to open and close the power generation circuit based on measurements of knee angle, and a knee brace to distribute the device reaction torque over

a large leg surface area. The device introduced in [17] selectively engages power generation towards the end of swing extension, assisting knee flexor muscles by producing substantial flexion torque (6.4 Nm), and converts the input mechanical power into electricity (54.6% efficiency). Consequently, six subjects walking at 1.5 m/s generate  $4.8 \pm 0.8$  W of electrical power with only a  $5.0 \pm 21$  W increase in metabolic cost. Figure 1.3 shows the model of this device.

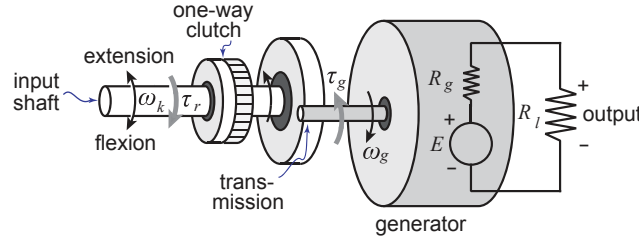


Figure 1.3: Simple model of the biomechanical energy harvester [18].

During walking, the foot moves both vertically and horizontally. The reported horizontal velocity of the heel stride resembles the positive part of a sine wave which starts at about 50% of the stride, ends at a full stride, and has a maximum value of a few meters per second. For a small load attached to the foot, this horizontal speed can be used to generate energy through a swing weight. Based on calculations in [19], foot swing has good potential as a power source. However, it does not provide a large direct force, which eliminates the application of piezoelectric and electroactive polymers.

This study focuses on center-of-mass motion. During walking, the hip, which coincides with the center of mass for the entire body, follows an up-and-down motion that resembles a sine wave [20]. This means that any object carried by a human will follow a similar trajectory. Hence, there should be a transfer of mechanical energy between load and body. If one is carrying a load in a backpack, because it is fixed to the body, it has to go up and down to follow the same trajectory. If the load is heavy, a significant amount of mechanical energy generated by muscles must be transferred. Although this represents a large potential source of mechanical energy, it is also inaccessible if the load is rigidly attached to the body [21]. We have focused on a device, the suspended-load backpack, that could be interposed between the body and the load, resulting in differential movement and the potential for generating

a considerable amount of electrical energy. The energy can be harvested with a magnetic actuation method. In [19], a linear permanent magnet coreless moving coil generator topology is proposed and a detailed design procedure is discussed. In lieu of using a linear permanent magnet generator, we use a permanent magnet brushless generator in this study. By utilizing some mechanical apparatus, the linear vertical motion of the backpack can be converted to a rotary one appropriate for use with the mentioned generator.

## 1.4 Outline of the Thesis

It is desired to build a device with higher output energy; i.e. the accumulated power should be as great as possible. In addition, the mass of the generator should be considered properly. Therefore, the magnetic generator should be optimized from different perspectives. In Chapter 2 of the thesis, fundamentals of permanent magnet brushless motors are discussed. Magnetic circuit model, flux linkage, back EMF, and torque are among the discussed topics. In Chapter 3, optimization of motor constant per unit volume of the motor is considered. A relatively simple model has been studied initially to obtain the optimal value of the split ratio to maximize the objective function. In further steps, we have made the model more detailed and accurate by considering the influence of tooth-tips and end-windings. Optimal solutions have been found analytically and different results are plotted. Conclusions are drawn in Chapter 4.

## CHAPTER 2

# BRUSHLESS PERMANENT MAGNET MOTOR

In this chapter, we study the fundamentals and design of brushless permanent magnet (BPM) motors. Because of their high efficiency, precise control, high speed operation, and compactness, these motors have received significant attention. One notable reason for the popularity of these machines is their construction consisting of permanent magnets built on the rotor and electrical windings on the stator. As the windings are stationary, no problematic electrical contacts, i.e., brushes, are needed. Moreover, it is easier to cool stationary windings. BPM machines can be built with any even number of magnet poles and any number of phases. Two- and three-phase motors are predominant because they minimize the number of power electronics devices used to control the winding currents.

The materials presented in this chapter are borrowed from [22]. The main purpose of this chapter is to give an introduction to this type of machine and its magnetic equivalent circuits. The reader is referred to the [22] for comprehensive coverage of this type of machine. The figures in this chapter are reproduced from [22]. This chapter summarizes the relevant material from [22].

### 2.1 Assumptions

Most BPM motors have magnets mounted on the rotor surface facing the air gap. In some others, the permanent magnets are buried in the steel structure. Generally three applications are assumed for the interior permanent magnet structures. First, flux concentration can be used by burying the magnets. Second, it is possible to run the motor in a wide speed range by using the method of field weakening control. Third, the presence of magnets in the steel allows the motor to operate at higher speeds.

## 2.2 Magnetic Circuit Model

The cross section of a BPM motor is shown in Figure 2.1. The rotor contains  $N_m = 4$  magnet poles facing the air gap. So,  $\theta_e = (N_m/2)\theta_m = 2\theta_m$  in which  $\theta_e$  and  $\theta_m$  are electrical and mechanical positions, respectively.

As shown in the figure, some magnet flux goes from one magnet to the next in the air gap without passing into the stator. The flux associated with this path is called *magnet leakage flux*.

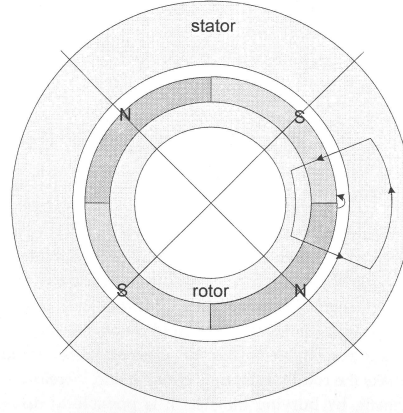


Figure 2.1: Fundamental motor structure and associated flux paths.

Figure 2.2 shows the magnetic equivalent circuit. The reluctances  $R_r$  and  $R_s$  are the rotor and rotor steel areas, respectively. The two half magnets are modeled as flux source  $\phi_r$  and associated magnet reluctance  $R_m$ , with the direction of the flux source dictating the magnet polarity. Primary flux flow from the magnets across the air gap into the stator is through the air gap reluctances denoted  $R_g$ .  $R_l$  is the leakage reluctance as flux passes from one magnet to the next. The fluxes of the circuit are the air gap flux  $\phi_g$ , the magnet flux  $\phi$ , and the leakage flux  $\phi_l$ .

In order to solve the magnetic circuit as shown in Figure 2.2, a simplification of the circuit is done with the result shown in Figure 2.3. The right magnet and rotor reluctance are in series with each other, so they are swapped in Figure 2.3(a). The rotor reluctance is next to the other reluctances and the two half magnets are next to each other. At this juncture, deriving an analytical expression for the leakage reluctance is not convenient. The air gap flux can be written in terms of the magnet flux as  $\phi_g = K_l\phi$ , where  $K_l$



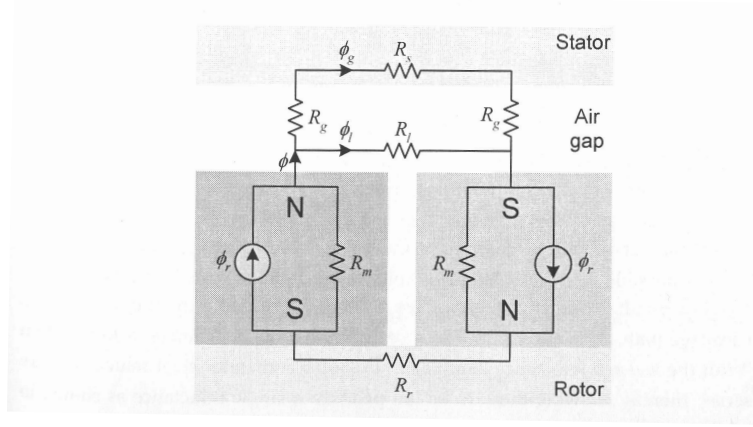


Figure 2.2: A magnetic circuit model for the structure shown in Figure 2.1.

is a *leakage factor*, which has a value less than one. Eliminating the leakage reluctance  $R_l$  as in Figure 2.3(b) can be done straightforwardly using the same equation. This is permissible as little flux flows in the leakage path. If the leakage reluctance is eliminated, the rotor and stator steel reluctances are in series, so they can be considered as a single reluctance as shown in Figure 2.3(b).

The two magnet halves in series in Figure 2.3(b) can be simplified as shown in Figure 2.3(c). Using the Norton equivalent circuit method, we can have the simplified magnet shown in Figure 2.3(c). The simplified flux source is  $\phi_r$ , and  $2R_m$  is the equivalent reluctance seen looking into the circuit. The two half magnets in series are like a single permanent magnet material with a doubled length,  $\phi_r$  remains unchanged but  $R_m$  doubles since reluctance is proportional to permanent material length.

Because of the saturation characteristic of ferromagnetic materials, the steel reluctance  $R_r + R_s$  is nonlinear in Figure 2.3(c). To find an analytic solution, the reluctance should be eliminated. Since permeability of the steel is higher than that of air, the steel reluctance is small in comparison with the air gap reluctance  $R_g$ , so the influence of the steel reluctance can be included in the air gap reluctance. That is, a *reluctance factor*  $K_r$  as shown in Figure 2.3(d) can be defined. This  $K_r$  is a constant greater than one that increases the air gap reluctance to compensate for the neglected steel reluctance.

It should be pointed out that, in practical situations, one hardly needs to obtain the analytical expressions for the leakage factor  $K_r$ . Their corresponding numerical values are usually determined based on the experience

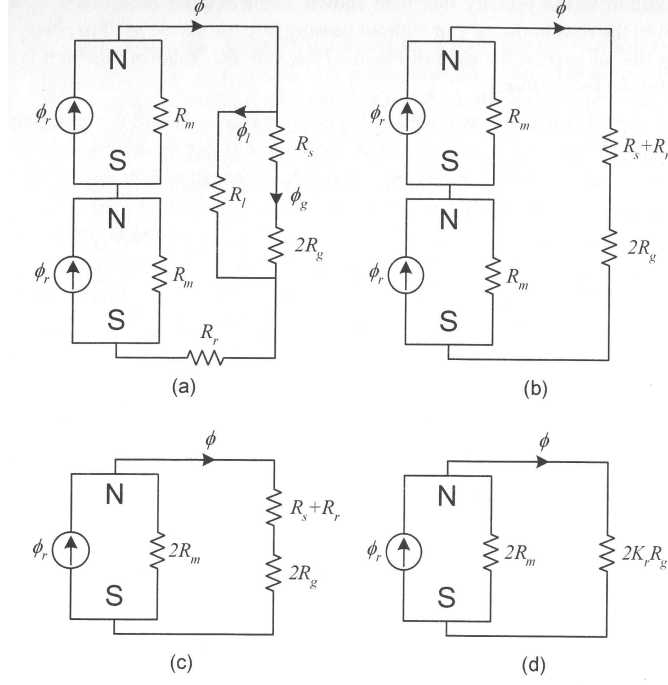


Figure 2.3: Simplifications of the magnetic circuit in Figure 2.2.

of the designer.

## 2.3 Magnetic Circuit Solution

Considering the magnetic circuit in Figure 2.3(d), the magnet flux  $\phi$  can be obtained using the same method of current division between resistors that is used in an electrical circuit:

$$\phi = \frac{2R_m}{2R_m + 2K_r R_g} \phi_r = \frac{1}{1 + K_r \frac{R_g}{R_m}} \phi_r \quad (2.1)$$

Based on  $\phi_g = K_l \phi$ , and general expressions for the magnet and air gap reluctances, i.e.,

$$R_m = \frac{l_m}{\mu_R \mu_0 A_m}, \quad R_g = \frac{g}{\mu_0 A_g} \quad (2.2)$$

the air gap flux can be expressed as

$$\phi = K_l \phi_r = \frac{K_l}{1 + K_r \frac{\mu_R g A_m}{l_m A_g}} \phi_r \quad (2.3)$$

where the magnet length and cross-sectional area are denoted by  $l_m$  and  $A_m$ , respectively, and  $g$  and  $A_g$  are the air gap length and cross-sectional area respectively. Substituting the *flux concentration factor*  $C_\phi = A_m/A_g$ , the flux density relationships  $B_g = \phi_g/A_g$  and  $B_r = \phi_r/A_m$ , and the permeance coefficient  $P_c = l_m/(gC_\phi)$  in the equation for  $\phi_g$  gives an air gap flux density of

$$B_g = \frac{K_l C_\phi}{1 + K_r \frac{\mu_R}{P_c}} B_r \quad (2.4)$$

Equation (2.4) shows the air gap flux density crossing the air gap. For motors equipped with surface magnets, the leakage factor is in the range  $0.9 \leq K_l < 1.0$  and the reluctance factor is in the range  $1.0 < K_r \leq 1.2$ .

## 2.4 Flux Linkage, Back EMF, and Torque

At this point, a full pitch winding is considered in a four-magnet ( $N_m = 4$ ) motor with  $N$  turns (Figure 2.4). The flux linkage in this winding facing the south pole is  $\lambda = -N\phi_g$ .

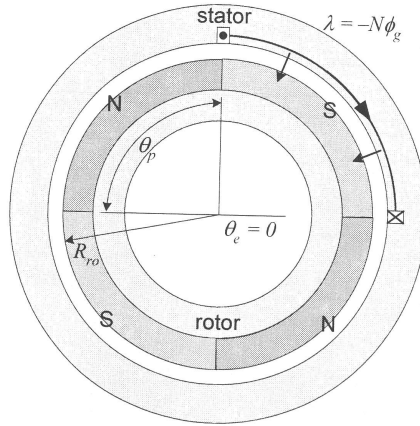


Figure 2.4: Motor having one full-pitch coil.

The flux linkage waveform is shown in Figure 2.5. The corresponding back EMF is the derivative of the waveform using Faraday's law. As the flux linkage is triangular, the back EMF has a square wave. The period of back EMF is 360 °E.

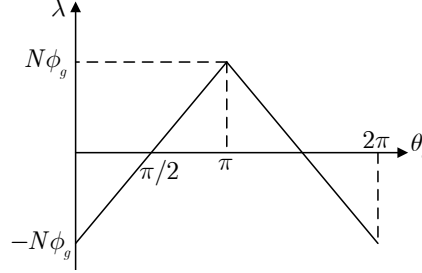


Figure 2.5: Flux linkage as a function of rotor position.

Analytically, the back EMF is given by

$$e_b = \frac{d\lambda}{dt} = \frac{d\theta_e}{dt} \frac{d\lambda}{d\theta_e} = \omega_e \frac{d\lambda}{d\theta_e} = \frac{N_m}{2} \omega_m \frac{d\lambda}{d\theta_e} = \frac{N_m}{2} \omega_m \frac{2N\phi_g}{\pi} \quad (2.5)$$

where  $\omega_m$  is the rotor mechanical speed in radM/s. In addition, the air gap flux can be expressed as

$$\phi_g = B_g A_g = B_g R_{ro} \theta_p L_{st} = \frac{2\pi}{N_m} B_g L_{st} R_{ro} \quad (2.6)$$

where  $B_g$  is the air gap flux density,  $\theta_p$  is the angular pole pitch in radM,  $R_{ro}$  is the air gap radius at the magnet surface, and  $L_{st}$  is the length of the machine. Substituting this relationship into (2.5) gives the amplitude of the back EMF  $E_b$ :

$$|e_b| = E_b = \frac{N_m}{2} \omega_m \frac{2N}{\pi} \left( \frac{2\pi}{N_m} B_g L_{st} R_{ro} \right) = 2N B_g L_{st} R_{ro} \omega_m = K_e \omega_m \quad (2.7)$$

This result is consistent with the  $Blv$  law. The factor  $2N$  is because of the two slots each having  $N$  conductors, and  $R_{ro}\omega_m$  is the linear velocity. All terms in the expression except for  $\omega_m$  form a *back EMF constant*  $K_e$ , whose units are V/(radM/s).

Using the formula  $e_b i = T\omega_m$  in Eqs. (2.5) and (2.7) yields the torque produced by a current  $i$  flowing in the coil. The amplitude of the torque is given by

$$|T| = \frac{E_b i}{\omega_m} = 2NB_g L_{st} R_{ro} i = K_t i \quad (2.8)$$

The terms in the Eq. (2.8) represent the force experienced by the rotor except the  $R_{ro}$ . This force acting at the radius  $R_{ro}$  gives the torque. In other words, except for  $i$ , all terms in Eq. (2.8) form a *torque constant*  $K_t$ . The torque constant and the back EMF constant described earlier are equal to each other, i.e.,

$$K_e = K_t = 2NB_g L_{st} R_{ro} \quad (2.9)$$

An ideal situation was considered to derive the analytical formulas for the flux, flux linkage, back EMF, and torque. In a practical situation, the air gap flux density does not have a square wave configuration. Consequently, the flux linkage does not have the ideal triangular shape and therefore the back EMF is not a square waveform. Rigorous mathematical analysis is required to determine the actual corresponding waveforms.

The preceding paragraphs discussed one full pitch coil. New coils can be added and connected together in series to shape the back EMF for the entire winding. Therefore, the back EMF amplitude can be written as

$$E_b = 2N_m NB_g L_{st} R_{ro} \omega_m \quad (2.10)$$

The amplitude of the torque multiplied by  $N_m$  is

$$|T| = 2N_m NB_g L_{st} R_{ro} i \quad (2.11)$$

This result is consistent with the formula  $T = kD^2L$  where  $T$  is torque,  $k$  is a constant,  $D$  is the rotor diameter, and  $L$  is the rotor length.

As mentioned previously, it is very uncommon to see a machine having more than three phases because of the number of power electronics devices used to control the winding currents. Using more than three phases is only justifiable at high power ranges.

## CHAPTER 3

# MOTOR CONSTANT OPTIMIZATION

In the preceding chapter, we focused on the fundamentals of BPM machines. In this chapter, we will concentrate on maximization of motor constant per unit volume of the machine. The motor constant shows torque efficiency, which is different from power efficiency [22]. According to [22], motor constant indicates how efficiently a motor generates torque as a function of the  $I^2R$  losses. In fact, motor constant is not only related to the desired motor output, but is also inversely proportional to the cost of producing that output. Hence, motor constant gives more valuable insight into maximizing motor performance in comparison with torque in [23]. We start with a simplified case and as we go further, we will consider more details in our problem.

### 3.1 Optimization of Motor Constant per Unit Volume

For the motor constant, we have [22]

$$K_m = \frac{B_g R_{ro}}{\sqrt{\rho}} \sqrt{V_{wb}} \quad (3.1)$$

where  $V_{wb}$  is the cross-sectional area of the conductors. For the  $V_{wb}$ , we have

$$V_{wb} = 2l_a A_{wb} \quad (3.2)$$

$$= 2l_a \frac{\frac{A_s}{2} K_s}{3 \frac{N_w}{N_s}} = 2l_a \frac{A_s}{2} K_s \frac{1}{3} \frac{N_s}{N_w} \quad (3.3)$$

$$= \frac{1}{3} l_a \frac{A_s K_s N_s}{N_w} \quad (3.4)$$

Also, we have  $R_{ro} + g = D_s/2$ . Since  $g \ll D_s/2$ , we can approximate  $R_{ro}$  as  $D_s/2$ . So the motor constant will become

$$K_m = \frac{B_g D_s}{2\sqrt{\rho}} \sqrt{\frac{l_a A_s K_s N_s}{3N_w}} \quad (3.5)$$

The equation for the motor constant per unit volume is

$$\frac{K_m}{V} = \frac{B_g D_s}{2\sqrt{\rho}} \frac{4}{\pi} \frac{1}{D_o^2 l_a} \sqrt{\frac{l_a A_s K_s N_s}{3N_w}} \quad (3.6)$$

$$= \frac{2B_g}{\pi\sqrt{\rho}} \frac{D_s}{D_o^2 l_a} \sqrt{\frac{l_a A_s K_s N_s}{3N_w}} \quad (3.7)$$

$$= \frac{2B_g}{\pi\sqrt{\rho}} \sqrt{\frac{D_s^2}{D_o^4} \frac{1}{l_a} \frac{A_s K_s N_s}{3N_w}} \quad (3.8)$$

Using the equation for  $A_s$

$$A_s = \frac{\pi D_o^2}{4N_s} \left\{ \left( \frac{D_s}{D_o} \right)^2 \left[ \frac{\pi}{3p} \left( \frac{\pi}{3p} + 2 \right) \left( \frac{B_g}{B_{max}} \right)^2 + 2 \frac{B_g}{B_{max}} - 1 \right] \right. \\ \left. - \left( \frac{D_s}{D_o} \right) \cdot 2 \left( \frac{\pi}{3p} + 1 \right) \left( \frac{B_g}{B_{max}} \right) + 1 \right\} \quad (3.9)$$

we have  $K_m/V$  as

$$\frac{K_m}{V} = \frac{2B_g}{\pi\sqrt{\rho}} \sqrt{\frac{\pi K_s}{12l_a N_w}} Q \quad (3.10)$$

where  $Q$  is

$$Q = \left( \frac{D_s}{D_o} \right)^4 \left[ \frac{\pi}{3p} \left( \frac{\pi}{3p} + 2 \right) \left( \frac{B_g}{B_{max}} \right)^2 + 2 \frac{B_g}{B_{max}} - 1 \right] \\ - \left( \frac{D_s}{D_o} \right)^3 \cdot 2 \left( \frac{\pi}{3p} + 1 \right) \left( \frac{B_g}{B_{max}} \right) + \left( \frac{D_s}{D_o} \right)^2 \quad (3.11)$$

So, the objective function is defined as

$$\frac{K_m}{V} = \frac{2B_g}{\pi\sqrt{\rho}} \sqrt{\frac{\pi K_s}{12l_a N_w}} \sqrt{ax^4 + bx^3 + x^2} \quad (3.12)$$

where

$$x = \frac{D_s}{D_o} \quad (3.13)$$

$$a = \frac{\pi}{3p} \left( \frac{\pi}{3p} + 2 \right) \left( \frac{B_g}{B_{max}} \right)^2 + 2 \frac{B_g}{B_{max}} - 1 \quad (3.14)$$

$$b = -2 \left( \frac{\pi}{3p} + 1 \right) \left( \frac{B_g}{B_{max}} \right) \quad (3.15)$$

By differentiating  $K_m/V$  relative to  $x$  and equating to zero, we get

$$4ax^3 + 3bx^2 + 2x = 0 \Rightarrow x(4ax^2 + 3bx + 2) = 0 \quad (3.16)$$

$$x = 0 \quad \text{or} \quad 2ax^2 + \left( \frac{3}{2} \right)bx + 1 = 0 \quad (3.17)$$

The solution to the above equation is

$$x = \frac{D_s}{D_o} = \frac{\left( -\frac{3}{2}b \right) - \sqrt{\left( -\frac{3}{2}b \right)^2 - 4(2a)}}{4a} \quad (3.18)$$

where

$$-\frac{3}{2}b = \left( -\frac{3}{2} \right) \left[ -2 \left( \frac{\pi}{3p} + 1 \right) \left( \frac{B_g}{B_{max}} \right) \right] \quad (3.19)$$

$$= 3 \left( \frac{\pi}{3p} + 1 \right) \left( \frac{B_g}{B_{max}} \right) \quad (3.20)$$

$$4a = 4 \left[ \frac{\pi}{3p} \left( \frac{\pi}{3p} + 2 \right) \left( \frac{B_g}{B_{max}} \right)^2 + 2 \frac{B_g}{B_{max}} - 1 \right] \quad (3.21)$$

$$= \frac{4\pi}{3p} \left( \frac{\pi}{3p} + 2 \right) \left( \frac{B_g}{B_{max}} \right)^2 + 8 \frac{B_g}{B_{max}} - 4 \quad (3.22)$$

The variation of optimal split ratio vs.  $B_g/B_{max}$  for different numbers of pole-pairs is shown in Figure 3.1.

It can be seen that as  $B_g/B_{max}$  is increased, the optimal split ratio reduces. It can also be seen from Figure 3.1 that, for a given ratio  $B_g/B_{max}$ , the optimal split ratio increases as the number of pole-pairs is increased. Figure 3.1 also shows that the influence of the pole number becomes more significant as the number of pole-pairs is reduced.



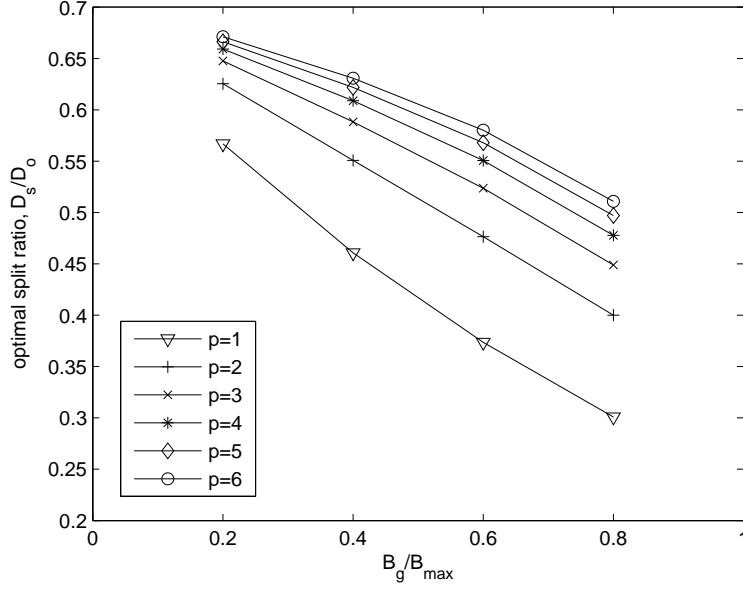


Figure 3.1: Variation of optimal split ratio  $B_g/B_{max}$  for motor with non-overlapping winding.

### 3.2 Influence of Winding Disposition on Optimal Split Ratio

In the preceding section, an analytical expression for the optimal split ratio was derived for a specific motor having a non-overlapping stator winding. In the subsequent sections, the analysis is done for an overlapping winding, a sinusoidal air gap flux density distribution and 180° electrical brushless AC operation.

For motors having a distributed overlapping winding, the number of series turns per phase  $N_w$  is replaced by the effective number of series turns per phase  $K_{dp}N_w$ , where  $K_{dp}$  is the winding factor. Therefore,  $V_{wb}$  can be written as

$$V_{wb} = 2l_a A_{cond} = 2l_a \frac{\frac{A_s}{2} K_s}{3 \frac{K_{dp} N_w}{N_s}} = \frac{1}{3} l_a \frac{A_s K_s N_s}{K_{dp} N_w} \quad (3.23)$$

Consequently, for the motor constant we have

$$K_m = \frac{B_g D_s}{2\sqrt{\rho}} \sqrt{\frac{l_a A_s K_s N_s}{3 K_{dp} N_w}} \quad (3.24)$$

The equation for motor constant per unit volume can be written as

$$\frac{K_m}{V} = \frac{B_g D_s}{2\sqrt{\rho}} \frac{4}{\pi} \frac{1}{D_o^2 l_a} \sqrt{\frac{l_a A_s K_s N_s}{3K_{dp} N_w}} \quad (3.25)$$

$$= \frac{2B_g D_s}{\pi\sqrt{\rho} D_o^2 l_a} \sqrt{\frac{l_a A_s K_s N_s}{3K_{dp} N_w}} \quad (3.26)$$

$$= \frac{2B_g}{\pi\sqrt{\rho}} \sqrt{\frac{D_s^2}{D_o^4} \frac{1}{l_a^2} \frac{l_a A_s K_s N_s}{3K_{dp} N_w}} \quad (3.27)$$

Substitution of  $A_s$  in  $K_m/V$  yields

$$\frac{K_m}{V} = \frac{2B_g}{\pi\sqrt{\rho}} \sqrt{\frac{\pi K_s}{12l_a K_{dp} N_w}} \sqrt{ax^4 + bx^3 + x^2} \quad (3.28)$$

By differentiating  $K_m/V$  relative to  $x$  and equating to zero, we get

$$4ax^3 + 3bx^2 + 2x = 0 \Rightarrow x(4ax^2 + 3bx + 2) = 0 \quad (3.29)$$

$$x = 0 \quad \text{or} \quad 2ax^2 + \left(\frac{3}{2}\right)bx + 1 = 0 \quad (3.30)$$

The solution to the above equation is

$$x = \frac{D_s}{D_o} = \frac{\left(-\frac{3}{2}b\right) - \sqrt{\left(\frac{3}{2}b\right)^2 - 4(2a)}}{4a} \quad (3.31)$$

where

$$-\frac{3}{2}b = \left(-\frac{3}{2}\right)\left[-2\left(\frac{\pi}{2p} + 1\right)\left(\frac{B_g}{B_{max}}\right)\right] \quad (3.32)$$

$$= 3\left(\frac{\pi}{2p} + 1\right)\left(\frac{B_g}{B_{max}}\right) \quad (3.33)$$

$$4a = 4\left[\frac{\pi}{2p}\left(\frac{\pi}{2p} + 2\right)\left(\frac{B_g}{B_{max}}\right)^2 + 2\frac{B_g}{B_{max}} - 1\right] \quad (3.34)$$

$$= \frac{2\pi}{p}\left(\frac{\pi}{2p} + 2\right)\left(\frac{B_g}{B_{max}}\right)^2 + 8\frac{B_g}{B_{max}} - 4 \quad (3.35)$$

Figure 3.2 compares optimal split ratios for motors having overlapping and non-overlapping windings.

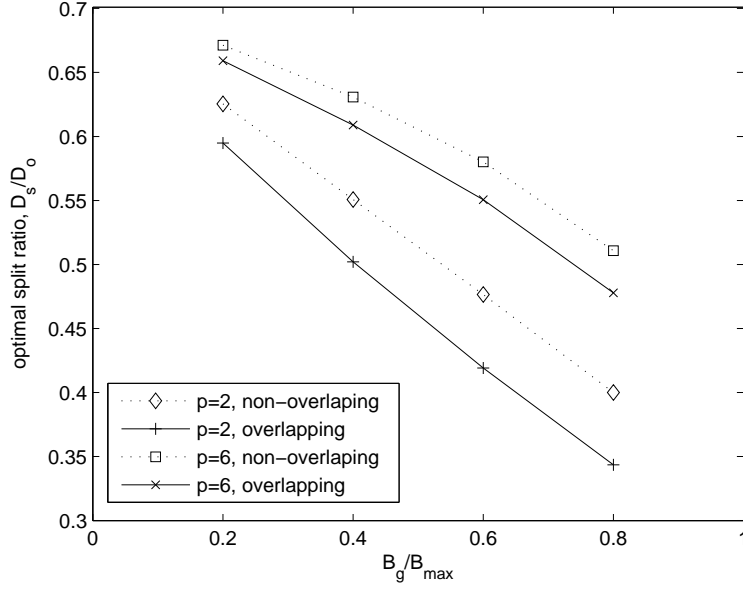


Figure 3.2: Variation of optimal split ratio with number of pole-pairs and winding disposition.

It can be concluded from the figure that the optimal split ratio in a motor with an overlapping winding is smaller than that for a motor with a non-overlapping winding.

### 3.3 Influence of Tooth-Tips on Optimal Split Ratio

In previous sections, the influence of both the stator tooth-tips and the end-windings has been neglected to simplify the derivation of analytical results. Nevertheless, tooth-tips are should be considered appropriately. They maximize the coil flux linkage and increase a high phase inductance. Considering rectangular tooth-tips, as shown in Figure 3.3, the stator slot area can be rewritten as

$$\begin{aligned}
 A_s = \frac{\pi D_o^2}{4N_s} \left\{ \left( \frac{D_s}{D_o} \right)^2 \left[ \frac{\pi}{3p} \left( \frac{\pi}{3p} + 2 \right) \left( \frac{B_g}{B_{max}} \right)^2 + 2 \frac{B_g}{B_{max}} - 1 \right] - \left( \frac{D_s}{D_o} \right) \times \right. \\
 \left. \left[ 2 \left( \frac{\pi}{3p} + 1 - 2 \frac{h_t}{D_o} \right) \left( \frac{B_g}{B_{max}} \right) + 4 \frac{h_t}{D_o} \right] + 1 - 4 \left( \frac{h_t}{D_o} \right)^2 \right\} \quad (3.36)
 \end{aligned}$$

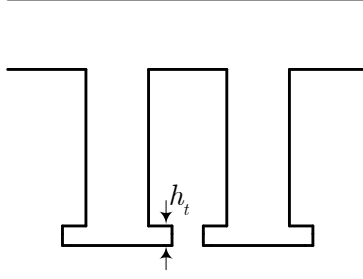


Figure 3.3: Idealized stator slot shape.

where  $h_t$  is the height of the tooth-tips.

For the  $K_m/V$ , we have

$$\frac{K_m}{V} = \frac{B_g D_s}{2\sqrt{\rho}} \sqrt{\frac{l_a A_s K_s N_s}{3N_w}} \quad (3.37)$$

Substitution of presented  $A_s$  in the last equation yields

$$\frac{K_m}{V} = \frac{2B_g}{\pi\sqrt{\rho}} \sqrt{\frac{\pi K_s}{12l_a N_w}} Q \quad (3.38)$$

where  $Q$  is defined as

$$\begin{aligned} Q = & \left(\frac{D_s}{D_o}\right)^4 \left[ \frac{\pi}{3p} \left( \frac{\pi}{3p} + 2 \right) \left( \frac{B_g}{B_{max}} \right)^2 + 2 \frac{B_g}{B_{max}} - 1 \right] \\ & - \left(\frac{D_s}{D_o}\right)^3 \left[ 2 \left( \frac{\pi}{3p} + 1 - 2 \frac{h_t}{D_o} \right) \left( \frac{B_g}{B_{max}} \right) + 4 \frac{h_t}{D_o} \right] \\ & + \left(\frac{D_s}{D_o}\right)^2 \left[ 1 - 4 \left( \frac{h_t}{D_o} \right)^2 \right] \end{aligned} \quad (3.39)$$

So the objective function is defined as

$$\frac{K_m}{V} = \frac{2B_g}{\pi\sqrt{\rho}} \sqrt{ax^4 + bx^3 + cx^2} \quad (3.40)$$

where

$$x = \frac{D_s}{D_o} \quad (3.41)$$

$$a = \frac{\pi}{3p} \left( \frac{\pi}{3p} + 2 \right) \left( \frac{B_g}{B_{max}} \right)^2 + 2 \frac{B_g}{B_{max}} - 1 \quad (3.42)$$

$$b = - \left[ 2 \left( \frac{\pi}{3p} + 1 - 2 \frac{h_t}{D_o} \right) \left( \frac{B_g}{B_{max}} \right) + 4 \frac{h_t}{D_o} \right] \quad (3.43)$$

$$c = 1 - 4 \left( \frac{h_t}{D_o} \right)^2 \quad (3.44)$$

In the applications that we are considering, the term  $h_t/D_o$  is negligible, so we can treat it as a constant value.

By differentiating  $K_m/V$  relative to  $x$  and equating to zero, we get

$$4ax^3 + 3bx^2 + 2cx = 0 \Rightarrow x(4ax^2 + 3bx + 2c) = 0 \quad (3.45)$$

$$x = 0 \quad \text{or} \quad 2ax^2 + \left( \frac{3}{2} \right)bx + c = 0 \quad (3.46)$$

The solution to the above equation is

$$x = \frac{D_s}{D_o} = \frac{\left( -\frac{3}{2}b \right) - \sqrt{\left( -\frac{3}{2}b \right)^2 - 4(2a)c}}{4a} \quad (3.47)$$

in which

$$4a = 4 \frac{k\pi}{p} \left( \frac{k\pi}{p} + 2 \right) \left( \frac{B_g}{B_{max}} \right)^2 + 8 \frac{B_g}{B_{max}} - 4 \quad (3.48)$$

and

$$-\frac{3}{2}b = 3 \left( \frac{k\pi}{p} + 1 - 2 \frac{h_t}{D_o} \right) \left( \frac{B_g}{B_{max}} \right) + 6 \frac{h_t}{D_o} \quad (3.49)$$

where  $k = 1/2$  for non-overlapping winding and  $k = 1/3$  for overlapping winding.

The influence of the tooth-tips on the optimal split ratios for a four-pole motor equipped with a non-overlapping winding is shown in Figure 3.4.

As can be seen, a tooth-tip height of 4 mm reduces the optimal split ratio by  $\sim 20\%$ .

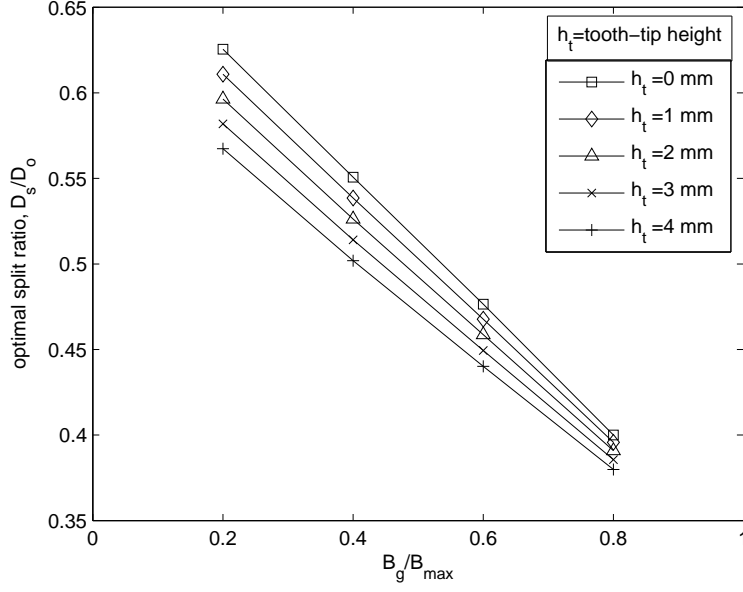


Figure 3.4: Influence of height of tooth tips on optimal split ratio  $p = 2$ ,  $D_o = 90$  mm, non-overlapping winding.

### 3.4 Influence of End-Windings on Optimal Split Ratio

We have the equation for the motor constant as

$$K_m = \frac{B_g R_{ro}}{\sqrt{\rho}} \sqrt{V_{wb}} \quad (3.50)$$

Length  $l_a$  in the equation  $V_{wb} = 2l_a A_{wb}$  can be replaced by  $l_a + l_e$ . Therefore

$$V_{wb} = 2(l_a + l_e) A_{cond} = 2(l_a + l_e) \frac{\frac{A_s}{2} K_s}{3 \frac{K_{dp} N_w}{N_s}} = \frac{1}{3} (l_a + l_e) \frac{A_s K_s N_s}{K_{dp} N_w} \quad (3.51)$$

The motor constant can be written as (using the approximation  $R_{ro} \approx D_s/2$ )

$$K_m = \frac{B_g D_s}{2\sqrt{\rho}} \sqrt{\frac{(l_a + l_e) A_s K_s N_s}{3 K_{dp} N_w}} \quad (3.52)$$

The motor constant per unit volume is

$$\begin{aligned}
\frac{K_m}{V} &= \frac{B_g D_s}{2\sqrt{\rho}} \frac{4}{\pi D_o^2 l_a} \sqrt{\frac{(l_a + l_e) A_s K_s N_s}{3 K_{dp} N_w}} \\
&= \frac{2B_g}{\pi\sqrt{\rho}} \sqrt{\frac{D_s^2}{D_o^4} \frac{1}{l_a^2} \frac{(l_a + l_e) A_s K_s N_s}{3 K_{dp} N_w}} \\
&= \frac{2B_g}{\pi l_a \sqrt{\rho}} \sqrt{\frac{\pi K_s}{12 K_{dp} N_w}} \sqrt{Q}
\end{aligned} \tag{3.53}$$

where

$$\begin{aligned}
Q &= (l_a + l_e) \frac{D_s^2}{D_o^2} \left\{ \left( \frac{D_s}{D_o} \right)^2 \left[ \frac{k\pi}{p} \left( \frac{k\pi}{p} + 2 \right) \left( \frac{B_g}{B_{max}} \right)^2 + 2 \frac{B_g}{B_{max}} - 1 \right] \right. \\
&\quad \left. - \left( \frac{D_s}{D_o} \right) \left[ 2 \left( \frac{k\pi}{p} + 1 - 2 \frac{h_t}{D_o} \right) \left( \frac{B_g}{B_{max}} \right) + 4 \frac{h_t}{D_o} \right] + 1 - 4 \left( \frac{h_t}{D_o} \right)^2 \right\} \\
&= (l_a + l_e) \left\{ \left( \frac{D_s}{D_o} \right)^4 \left[ \frac{k\pi}{p} \left( \frac{k\pi}{p} + 2 \right) \left( \frac{B_g}{B_{max}} \right)^2 + 2 \frac{B_g}{B_{max}} - 1 \right] \right. \\
&\quad \left. - \left( \frac{D_s}{D_o} \right)^3 \left[ 2 \left( \frac{k\pi}{p} + 1 - 2 \frac{h_t}{D_o} \right) \left( \frac{B_g}{B_{max}} \right) + 4 \frac{h_t}{D_o} \right] + \left( \frac{D_s}{D_o} \right)^2 \left[ 1 - 4 \left( \frac{h_t}{D_o} \right)^2 \right] \right\}
\end{aligned} \tag{3.54}$$

The objective function will be

$$\frac{K_m}{V} = \frac{2B_g}{\pi l_a \sqrt{\rho}} \sqrt{\frac{\pi K_s}{12 K_{dp} N_w}} \sqrt{(dx + e)(ax^4 + bx^3 + cx^2)} \tag{3.55}$$

where

$$x = \frac{D_s}{D_o} \tag{3.56}$$

$$\begin{aligned}
a &= \frac{k\pi}{p} \left( \frac{k\pi}{p} + 2 \right) \left( \frac{B_g}{B_{max}} \right)^2 + 2 \frac{B_g}{B_{max}} - 1 \\
b &= - \left[ 2 \left( \frac{k\pi}{p} + 1 - 2 \frac{h_t}{D_o} \right) \left( \frac{B_g}{B_{max}} \right) + 4 \frac{h_t}{D_o} \right] \\
c &= 1 - 4 \left( \frac{h_t}{D_o} \right)^2
\end{aligned} \tag{3.57}$$

$$k = \frac{1}{3} \quad (3.58)$$

$$d = \frac{\pi^2 D_o}{4N_s} \left[ \frac{1}{2} + \left(1 - \frac{\pi}{2N_s}\right) \frac{B_g}{B_{max}} \right] \quad (3.59)$$

$$e = l_a + \frac{\pi^2 D_o}{4N_s} \left[ \frac{1}{2} + \frac{h_t}{D_o} \right] \quad (3.60)$$

for non-overlapping winding and

$$k = \frac{1}{2} \quad (3.61)$$

$$d = \frac{3\pi^2 D_o}{2N_s} \left[ \frac{1}{2} - \frac{3\pi}{2N_s} \frac{B_g}{B_{max}} \right] \quad (3.62)$$

$$e = l_a + \frac{3\pi^2 D_o}{2N_s} \left[ \frac{1}{2} + \frac{h_t}{D_o} \right] \quad (3.63)$$

for overlapping winding.

By differentiating  $K_m/V$  relative to  $x$  and equating to zero, we get

$$x[(5ad)x^3 + 4(bd + af)x^2 + 3(cd + bf)x + 2cf] = 0 \quad (3.64)$$

A trivial solution to this equation is  $x = 0$ . We consider the third-degree polynomial

$$(5ad)x^3 + 4(bd + af)x^2 + 3(bf + cd)x + 2cf = 0 \quad (3.65)$$

Dividing the (3.65) by the leading coefficient, a monic polynomial results

$$x^3 + \frac{4(bd + af)}{5ad}x^2 + \frac{3(bf + cd)}{5ad}x + \frac{2cf}{5ad} = 0 \quad (3.66)$$

Using the method of solving third-degree monic polynomials, we have

$$m = 2 \left[ \frac{4(bd + af)}{5ad} \right]^3 - 9 \left[ \frac{4(bd + af)}{5ad} \right] \left[ \frac{3(cd + bf)}{5ad} \right] + \frac{54cf}{5ad} \quad (3.67)$$

$$k = \left[ \frac{4(bd + af)}{5ad} \right]^2 - 3 \left[ \frac{3(cd + bf)}{5ad} \right] \quad (3.68)$$

$$(3.69)$$



and

$$n = m^2 - 4k^3 \quad (3.70)$$

$$\omega = -\frac{1}{2} + \frac{\sqrt{3}}{2}i \quad (3.71)$$

$$\omega^2 = -\frac{1}{2} - \frac{\sqrt{3}}{2}i \quad (3.72)$$

The solutions to the equation are

$$x_1 = -\frac{1}{3} \left( \frac{4(bd + af)}{5ad} + \sqrt[3]{\frac{m + \sqrt{n}}{2}} + \sqrt[3]{\frac{m - \sqrt{n}}{2}} \right) \quad (3.73)$$

$$x_2 = -\frac{1}{3} \left( \frac{4(bd + af)}{5ad} + \omega^2 \sqrt[3]{\frac{m + \sqrt{n}}{2}} + \omega \sqrt[3]{\frac{m - \sqrt{n}}{2}} \right) \quad (3.74)$$

$$x_3 = -\frac{1}{3} \left( \frac{4(bd + af)}{5ad} + \omega \sqrt[3]{\frac{m + \sqrt{n}}{2}} + \omega^2 \sqrt[3]{\frac{m - \sqrt{n}}{2}} \right) \quad (3.75)$$

We can define  $q_1$  as

$$q_1 = \frac{1}{27}m = \frac{2(4af + 4bd)^2}{27(5ad)^3} - \frac{9(4af + 4bd)(3bf + 3cd)}{27(5ad)^2} + \frac{2cf}{5ad} \quad (3.76)$$

and  $p_1$  can be defined as

$$p_1 = -\frac{1}{9} \left( \frac{4(bd + af)}{5ad} \right)^2 + \frac{cd + bf}{5ad} \quad (3.77)$$

$$k = \frac{(4ae + 2bd)^2}{(3ad)^2} - \frac{3be + cd}{ad} = 3 \left[ \frac{(4ae + 2bd)^2}{3(3ad)^2} - \frac{3be + cd}{3ad} \right] = -3p_1 \quad (3.78)$$

$$\begin{aligned} \frac{1}{4} \frac{1}{(27)^2} n &= \frac{1}{4} \frac{1}{(27)^2} (m^2 - 4k^3) = \frac{1}{2^2} \left( \frac{m}{27} \right)^2 + \left( \frac{-k}{3^2} \right)^3 \\ &= \left( \frac{q_1}{2} \right)^2 + p_1^3 \end{aligned} \quad (3.79)$$

Based on the parameters calculated above, we can simplify the solutions to the cubic polynomial:

$$\begin{aligned}
x_1 &= -\frac{4ae + 2bd}{9ad} + \left(-\frac{1}{3}\right)\sqrt[3]{\frac{m + \sqrt{n}}{2}} + \left(-\frac{1}{3}\right)\sqrt[3]{\frac{m - \sqrt{n}}{2}} \\
&= -\frac{4ae + 2bd}{9ad} + \sqrt[3]{-\frac{1}{27}\frac{m}{2} - \frac{1}{27}\frac{\sqrt{n}}{2}} + \sqrt[3]{-\frac{1}{27}\frac{m}{2} + \frac{1}{27}\frac{\sqrt{n}}{2}} \\
&= -\frac{4ae + 2bd}{9ad} + \sqrt[3]{-\frac{1}{27}\frac{m}{2} - \sqrt{\frac{1}{4}\frac{1}{27^2}n}} + \sqrt[3]{-\frac{1}{27}\frac{m}{2} + \sqrt{\frac{1}{4}\frac{1}{27^2}n}}
\end{aligned} \tag{3.80}$$

$$\begin{aligned}
x_2 &= -\frac{4ae + 2bd}{9ad} + \left(-\frac{1}{3}\right)\omega^2\sqrt[3]{\frac{m + \sqrt{n}}{2}} + \left(-\frac{1}{3}\right)\omega\sqrt[3]{\frac{m - \sqrt{n}}{2}} \\
&= -\frac{4ae + 2bd}{9ad} + \omega^2\sqrt[3]{-\frac{1}{27}\frac{m}{2} - \frac{1}{27}\frac{\sqrt{n}}{2}} + \omega\sqrt[3]{-\frac{1}{27}\frac{m}{2} + \frac{1}{27}\frac{\sqrt{n}}{2}} \\
&= -\frac{4ae + 2bd}{9ad} + \omega^2\sqrt[3]{-\frac{1}{27}\frac{m}{2} - \sqrt{\frac{1}{4}\frac{1}{27^2}n}} + \omega\sqrt[3]{-\frac{1}{27}\frac{m}{2} + \sqrt{\frac{1}{4}\frac{1}{27^2}n}}
\end{aligned} \tag{3.81}$$

$$\begin{aligned}
x_3 &= -\frac{4ae + 2bd}{9ad} + \left(-\frac{1}{3}\right)\omega\sqrt[3]{\frac{m + \sqrt{n}}{2}} + \left(-\frac{1}{3}\right)\omega^2\sqrt[3]{\frac{m - \sqrt{n}}{2}} \\
&= -\frac{4ae + 2bd}{9ad} + \omega\sqrt[3]{-\frac{1}{27}\frac{m}{2} - \frac{1}{27}\frac{\sqrt{n}}{2}} + \omega^2\sqrt[3]{-\frac{1}{27}\frac{m}{2} + \frac{1}{27}\frac{\sqrt{n}}{2}} \\
&= -\frac{4ae + 2bd}{9ad} + \omega\sqrt[3]{-\frac{1}{27}\frac{m}{2} - \sqrt{\frac{1}{4}\frac{1}{27^2}n}} + \omega^2\sqrt[3]{-\frac{1}{27}\frac{m}{2} + \sqrt{\frac{1}{4}\frac{1}{27^2}n}}
\end{aligned} \tag{3.82}$$

The optimal split ratio for motor constant per unit volume can be written as

$$\frac{D_s}{D_o} = y_i - \frac{4(bd + af)}{15ad}, \text{ where } i = 1, 2, 3 \tag{3.83}$$

$$y_1 = \sqrt[3]{-\frac{q_1}{2} - \sqrt{(\frac{q_1}{2})^2 + p_1^3}} + \sqrt[3]{-\frac{q_1}{2} + \sqrt{(\frac{q_1}{2})^2 + p_1^3}} \quad (3.84)$$

$$y_2 = \omega^2 \sqrt[3]{-\frac{q_1}{2} - \sqrt{(\frac{q_1}{2})^2 + p_1^3}} + \omega \sqrt[3]{-\frac{q_1}{2} + \sqrt{(\frac{q_1}{2})^2 + p_1^3}} \quad (3.85)$$

$$y_3 = \omega \sqrt[3]{-\frac{q_1}{2} - \sqrt{(\frac{q_1}{2})^2 + p_1^3}} + \omega^2 \sqrt[3]{-\frac{q_1}{2} + \sqrt{(\frac{q_1}{2})^2 + p_1^3}} \quad (3.86)$$

$$(3.87)$$

where

$$\omega = -\frac{1}{2} + \frac{\sqrt{3}}{2}i \quad (3.88)$$

$$p_1 = -\frac{1}{9} \left( \frac{4(bd + af)}{5ad} \right)^2 + \frac{cd + bf}{5ad} \quad (3.89)$$

$$q_1 = \frac{m}{27} = \frac{2(4af + 4bd)^2}{27(5ad)^3} - \frac{9(4af + 4bd)(3bf + 3cd)}{27(5ad)^2} + \frac{2cf}{5ad} \quad (3.90)$$

$$\begin{aligned} a &= \frac{k\pi}{p} \left( \frac{k\pi}{p} + 2 \right) \left( \frac{B_g}{B_{max}} \right)^2 + 2 \frac{B_g}{B_{max}} - 1 \\ b &= - \left[ 2 \left( \frac{k\pi}{p} + 1 - 2 \frac{h_t}{D_o} \right) \left( \frac{B_g}{B_{max}} \right) + 4 \frac{h_t}{D_o} \right] \\ c &= 1 - 4 \left( \frac{h_t}{D_o} \right)^2 \end{aligned} \quad (3.91)$$

and

$$k = \frac{1}{3} \quad (3.92)$$

$$d = \frac{\pi^2 D_o}{4N_s} \left[ \frac{1}{2} + \left( 1 - \frac{\pi}{2N_s} \right) \frac{B_g}{B_{max}} \right] \quad (3.93)$$

$$e = \frac{\pi^2 D_o}{4N_s} \left[ \frac{1}{2} + \frac{h_t}{D_o} \right] \quad (3.94)$$

$$f = e + l_a \quad (3.95)$$

for non-overlapping winding and

$$k = \frac{1}{2} \quad (3.96)$$

$$d = \frac{3\pi^2 D_o}{2N_s} \left[ \frac{1}{2} - \frac{3\pi}{2N_s} \frac{B_g}{B_{max}} \right] \quad (3.97)$$

$$e = \frac{3\pi^2 D_o}{2N_s} \left[ \frac{1}{2} + \frac{h_t}{D_o} \right] \quad (3.98)$$

$$f = e + l_a \quad (3.99)$$

for overlapping winding.

We have three solutions to the considered cubic polynomial, a feasible value for the optimal split ratio  $D_s/D_o$  being a real value in the range  $0 < D_s/D_o < 1$ .

Figures 3.5 and 3.6 compare the optimal split ratio for motors with non-overlapping and overlapping windings, both with and without a consideration of the end-windings.

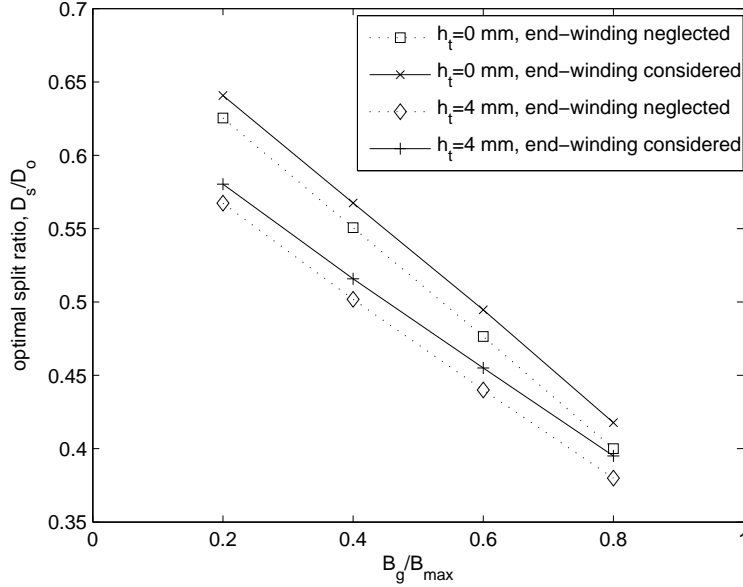


Figure 3.5: Influence of tooth-tips and end-winding on optimal split ratio.  $p = 2$ ,  $N_s = 6$ ,  $D_o = 90$  mm,  $l_a = 50$  mm, non-overlapping winding.

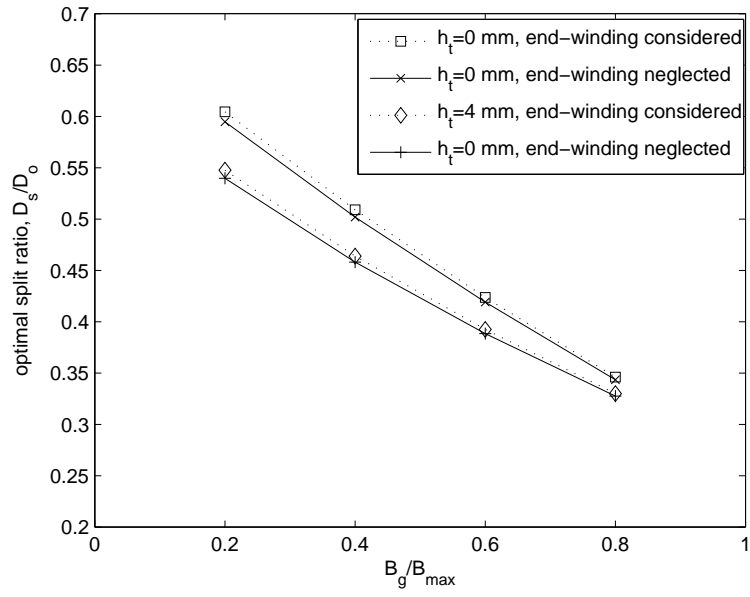


Figure 3.6: Influence of tooth-tips and end-winding on optimal split ratio.  
 $p = 2$ ,  $N_s = 12$ ,  $D_o = 90$  mm,  $l_a = 50$  mm, overlapping winding.

# CHAPTER 4

## CONCLUSION

This study focused on exploiting center-of-mass motion as a promising candidate for energy harvesting applications. During walking, the hip, where the center of mass for the entire body is located, follows an up-and-down course of motion, so any object carried by a human will follow a similar trajectory. To take advantage of this, there should be a transfer of mechanical energy between load and body. Based on the characteristics of motion, a brushless permanent magnet generator was chosen as the candidate for this energy conversion, rather than the linear permanent magnet generator used previously in the literature.

It is desired to build a device with higher output energy; i.e. the accumulated power should be as high as possible. In addition, the mass of the generator should be considered carefully because it will be mounted in a backpack. Therefore, the magnetic generator should be optimized from different perspectives. The split ratio, i.e. the ratio of the stator bore diameter to the stator outer diameter ( $D_s/D_o$ ), is considered as an important design parameter for permanent magnet (PM) brushless motors since it has a big influence on the torque capability and efficiency. Optimization of motor constant per unit volume as a function of split ratio was particularly considered. As pointed out previously, motor constant describes how efficiently a motor produces torque as a function of the  $I^2R$  losses incurred in the production of that torque. That is, motor constant is not only related to the desired motor output, but also inversely proportional to the cost of producing that output. Thus, motor constant provides more valuable insight into maximizing motor performance, which is the main purpose of this study. A relatively simple model was studied in earlier steps to obtain the optimal value of the split ratio to maximize the objective function. In further steps, we made the model more sophisticated by considering the influence of tooth-tips and end-windings. Optimal solutions were found analytically and different graphs

were plotted based on accomplished results.

It is concluded that maximizing the motor constant (as an indication of torque efficiency) per unit volume is a superior strategy to maximizing torque per unit volume, as is done in the literature to date.

## REFERENCES

- [1] J. Kymissis, C. Kendall, J. Paradiso, and N. Gershenfeld, "Parasitic power harvesting in shoes," in *Second International Symposium on Wearable Computers*, 1998, pp. 132-139.
- [2] T. Starner, "Human-powered wearable computing," *IBM Systems Journal*, vol. 35, nos. 3&4, pp. 618-629, 1996.
- [3] P. Niu, P. L. Chapman, R. Riemer, and X. Zhang, "Evaluation of motions and actuation methods for biomechanical energy harvesting," in *IEEE 35th Annual Power Electronics Specialists Conference*, vol. 3, 2004, pp. 2100-2106.
- [4] J. Alper, "The battery: Not yet a terminal case," *Science*, vol. 296, pp. 1224-1226, 2002.
- [5] R. F. Service, "Shrinking fuel cells promise power in your pocket," *Science*, vol. 296, pp. 1222-1224, 2002.
- [6] B. Kuhn and P. L. Chapman, "Harvesting walking energy for mobile electronics," National Science Foundation proposal, 2006.
- [7] H. A. Sodano, D. J. Inman, and G. Park, "A review of power harvesting from vibration using piezoelectric materials," *The Shock and Vibration Digest*, vol. 36, no. 3, pp. 197-205, 2004.
- [8] N. S. Shenck, "A demonstration of useful electric energy generation from piezoceramics in a shoe," M.S. thesis, Media Lab, Massachusetts Institute of Technology, Cambridge, MA, 1999.
- [9] N. S. Shenck and J. A. Paradiso, "Energy scavenging with shoe-mounted piezoelectrics," *IEEE Micro*, vol. 21, pp. 30-42, 2001.
- [10] J. P. Marsden and S. R. Montgomery, "Plantar power for arm prosthesis using body weight transfer," in *Human Locomotor Engineering*. London, England: Institute of Mechanical Engineers Press, 1971, pp. 277-282.
- [11] M. Umeda, K. Nakamura, and S. Ueha, "Analysis of transformation of mechanical impact energy to electrical energy using a piezoelectric



- vibrator,” *Japanese Journal of Applied Physics*, vol. 35, pp. 3267-3273, 1996.
- [12] N. G. Elvin, A. A. Elvin, and M. Spector, “A self-powered mechanical strain energy sensor,” *Smart Materials and Structures*, vol. 10, pp. 293-299, 2001.
  - [13] A. Kasyap, J. Lim, D. Johnson, S. Horowitz, T. Nishida, K. Ngo, M. Sheplak, and L. Cattafesta, “Energy reclamation from a vibrating piezo-ceramic composite beam,” in *Proceedings of the Ninth International Congress on Sound and Vibration*, 2002, pp. 36-43.
  - [14] R. Margaria, “Positive and negative work performances and their efficiencies in human locomotion,” *European Journal of Applied Physiology and Occupational Physiology*, vol. 25, no. 4, pp. 339-351, 1968.
  - [15] G. A. Brooks, T. D. Fahey, and K. M. Baldwin, *Exercise Physiology: Human Bioenergetics and Its Applications*, 4th ed. Boston, MA: McGraw-Hill, 2005.
  - [16] J. A. Paradiso and T. Starner, “Energy scavenging for mobile and wireless electronics,” *IEEE Pervasive Computing*, vol. 4, pp. 18-27, 2005.
  - [17] Q. Li, V. Naing, and J. M. Donelan, “Development of a biomechanical energy harvester,” *Journal of NeuroEngineering and Rehabilitation*, vol. 6, pp. 6-22, June 2009.
  - [18] J. M. Donelan, Q. Li, V. Naing, J. A. Hoffer, D. J. Weber, and A. D. Kuo, “Biomechanical energy harvesting: Generating electricity during walking with minimal user effort,” *Science*, vol. 319, pp. 807-810, 2008.
  - [19] P. Niu, “Biomechanical energy conversion,” Ph.D. dissertation, University of Illinois at Urbana-Champaign, Urbana, IL, 2007.
  - [20] S. A. Gard, S. C. Miff, and A. D. Kuo, “Comparison of kinematic and kinetic methods for computing the vertical motion of the body center of mass during walking,” *Human Movement Science*, vol. 22, pp. 597-610, 2004.
  - [21] L. C. Rome, L. Flynn, E. M. Goldman, and T. D. Yoo, “Generating electricity while walking with loads,” *Science*, vol. 309, pp. 1725-1728, 2005.
  - [22] D. C. Hanselman, *Brushless Permanent Magnet Motor Design*, 2nd ed. Cranston, RI: The Writers’ Collective, 2003.
  - [23] Y. Pang, Z. Q. Zhu, and D. Howe, “Analytical determination of optimal split ratio for permanent magnet brushless motors,” *IEE Proceedings Electric Power Application*, vol. 153, no. 1, pp. 7-13, Jan. 2006.

## AUTHOR'S BIOGRAPHY

Arash Sayyah was born in Shiraz, known as a beautiful and historic city located in the southwest of Iran. He passed his preschool education, elementary school and guidance school with the best educational achievements in Tehran. In 1997, he was admitted to Nikan high school, one of the largest and most luxurious schools in the country. He received his diploma with high distinction in mathematics and physics in 2001 from the same school. He received his B.S. degree in electrical engineering from the Shahid Beheshti University, Tehran, Iran, in 2007. He was admitted to the University of Illinois at Urbana-Champaign (UIUC) in January 2008, and will receive his M.S. degree in electrical engineering in May 2010 under supervision of Professor Patrick L. Chapman.

During his undergraduate study, he was involved in different research projects in the areas of power and control. The projects included optimization of harmonic losses in high-power electric machines, and application of the harmonic elimination technique in optimal PWM feeding schemes in high power applications. Furthermore, in one project, he considered minimization of current harmonic losses of a typical high power synchronous machine by developing a current tracking control method to suppress the detrimental transient conditions caused by step changes in the optimal pulse pattern trajectories. Experimental results corroborated the efficacy of the proposed method.

His graduate work at UIUC has focused on the development of biomechanical energy harvesting devices, minimization of the parasitic weight of designed devices, and optimizing the effects of human loading such as carrying efficiency. He has been a teaching assistant for Electric Machinery (ECE 431) and Senior Design Project Laboratory (ECE 445) in Spring 2010 and Fall 2009, respectively.